Growth of (Sr,La)-(Ta,Ti)-O-N perovskite oxide and oxynitride films by radio frequency magnetron sputtering: Influence of the reactive atmosphere on the film structure

Claire Le Paven, Laurent Le Gendre, Ratiba Benzerga, François Cheviré, F. Tessier, S. Jacq, S. Traoré-Mantion, Ala Sharaiha

Growth of (Sr,La)-(Ta,Ti)-O-N perovskite oxide and oxynitride films by radio frequency magnetron sputtering: influence of the reactive atmosphere on the film structure

C. Le Paven[a,*], *L. Le Gendre*[a], *R. Benzerga*[a], *F. Cheviré*[b], *F. Tessier*[b], *S. Jacq*[a], *S. Traoré-Mantion*[a], *A. Sharaiha*[a]

[a] Institut d'Electronique et de Télécommunications de Rennes (IETR, UMR-CNRS 6164), Equipe Matériaux Fonctionnels, IUT Saint Brieuc, Université de Rennes 1, 22000 Saint Brieuc, France

[b] Institut des Sciences Chimiques de Rennes (ISCR, UMR-CNRS 6226), Equipe Verres et Céramiques, Université de Rennes 1, 35042 Rennes, France

* Corresponding author: claire.lepave@nniv-rennes1.fr ; (33)-296609659

ABSTRACT

In the search for new dielectric and ferroelectric compounds, we were interested in the perovskite $(Sr_{1-x}La_x)_2(Ta_{1-x}Ti_x)_2O_7$ solid solution with ferroelectric end members $Sr_2Ta_2O_7$ (T_{Curie} = -107°C) and $La_2Ti_2O_7$ (T_{Curie} = 1461°C). In order to achieve a Curie temperature close to room temperature, the formulation with x = 0.01 was chosen and synthetized as thin films by reactive radio-frequency magnetron sputtering. In oxygen rich plasma, a $(Sr_{0.99}La_{0.01})_2(Ta_{0.99}Ti_{0.01})_2O_7$ film is deposited, characterized by a band-gap E_g = 4.75 eV and

an (110) epitaxial growth on (001)MgO substrate. The use of nitrogen rich plasma allows to synthesize $(Sr_{0.99}La_{0.01})(Ta_{0.99}Ti_{0.01})O_2N$ oxynitride films, with band gap E_g ~ 2.10 eV and a polycrystalline, textured or epitaxial growth on (001)MgO substrate. Nitrogen-substoichiometric oxynitride films with larger lattice cells are produced for low dinitrogen percentages in the sputtering plasma.

KEYWORDS

A3. Physical vapor deposition processes; A3. Perovskites; A3. Nitrides; A3. Oxides; B2. Dielectric materials; A1. X-ray diffraction

1. INTRODUCTION

For many years, perovskite materials have been studied regarding the wide variety of their properties achieved by substitutions on A and B cations-sites in the basic ABO_3 structure. Moreover, by replacing nitrogen for oxygen, oxynitride perovskite compounds were also synthesized [1]. They present original properties compared to their parent oxides, such as an absorption in the visible region resulting in colored materials with potential applications in the fields of visible light-driven photocatalysis [2,3] and pigments [4,5], or very high permittivities ranging from some tens to several thousands [6-8]. The dielectric behavior of perovskite oxynitrides is currently the subject of many studies; a relaxor-type ferroelectric behavior has been proposed, which would originate from an O/N order in the perovskite structure [9-11].

We have already reported on $LaTiO_2N$ perovskite oxynitride material synthesis and its dielectric characterization in low and high frequencies. Because of the specific difficulties encountered in the sintering of oxynitride materials [6,12], thin films deposition appears as a

reasonable alternative to provide dense samples on which measurements are possible. Furthermore, thin films can be easily integrated in planar devices. $LaTiO_2N$ films were obtained by reactive sputtering deposition of an oxynitride [13] or an oxide [14] target. In both cases, the use of nitrogen rich plasma was necessary to produce oxynitride films. Despite their high permittivities, $LaTiO_2N$ thin films did not show any ferroelectric behavior similar to the one of the oxide $La_2Ti_2O_7$ parent [15]. Considering that $La_2Ti_2O_7$ has a very high Curie temperature (T_C = 1461°C) [16], our approach was to combine it with $Sr_2Ta_2O_7$, a ferroelectric analog that exhibits a low Curie temperature (T_C = -107°C) [15], in order to synthetize a ferroelectric oxide with a T_C value close to the ambient temperature and thus benefit from high values of permittivities. From the work of Nanamastu on solid solutions $(1-x)Sr_2Ta_2O_7$-$xLa_2Ti_2O_7$ [15], we have extrapolated the evolution of T_C in function of x and selected x ~ 0.01 (1 %) for a T_C close to room temperature. This corresponds to the composition $(Sr_{0.99}La_{0.01})_2(Ta_{0.99}Ti_{0.01})_2O_7$; the oxynitride parent is $(Sr_{0.99}La_{0.01})(Ta_{0.99}Ti_{0.01})O_2N$. The present article deals with the synthesis and structural characterization of these oxide and oxynitride materials as thin films. Future research will report on their dielectric and ferroelectric characterization.

The depositions were performed by reactive radio-frequency magnetron sputtering using the oxide target sputtered under oxygen or nitrogen rich plasma. The influence of the reactive gas on the structural, morphological and optical characteristics was investigated. Since the targeted composition is not reported in literature, our work is compared to the deposition of related compounds: $Sr_2(Ta,Nb)_2O_7$ deposited by chemical route [17], $Sr_2Ta_2O_7$ elaborated by chemical route [18-20] or atomic vapor deposition [21-23] and $SrTaO_2N$ thin films deposited by nitrogen-plasma assisted pulsed laser deposition [24]. In the present study, films were deposited on single crystalline (001)MgO substrate. The mismatch between $Sr_2Ta_2O_7$ (pseudo-cubic, c_{PC} = 4.025 Å (JCPDS 72-0921) or $SrTaO_2N$ (pseudo-cubic, c_{PC} =

4.045 Å JCPDS 79-1311) and MgO (cubic, a = 4.211 Å) are, respectively, - 4.4 % and - 3.9 %, relatively low values to consider an oriented or epitaxial growth of samples.

2. MATERIAL AND METHODS

The deposition of films was made by reactive radio frequency magnetron sputtering in a Plassys MP450S reactor using an oxide target with the $(Sr_{0.99}La_{0.01})_2(Ta_{0.99}Ti_{0.01})_2O_7$ composition. The powdered target was obtained by solid state chemistry from the reactants $SrCO_3$, Ta_2O_5, La_2O_3 and TiO_2 weight in stoichiometric amounts and heated under air at 1400°C during 15 h. The formation of the oxide perovskite material was confirmed from X-Ray Diffraction (XRD) analysis, with all diffracted peaks assigned to a $Sr_2Ta_2O_7$-type structure with the $Cmc2_1$ space group (ferroelectric phase, JCPDS 72-0921). The EDS analysis gave a ratio Sr/Ta = 1.0. The 75 mm (3 inches) diameter target was shaped by uniaxial compaction of the powder at room temperature, and placed in the sputtering chamber.

Concerning the deposition, the reactive gas mixture (Ar + O_2 or Ar + N_2) was introduced in the chamber once the base pressure reached a value of 10^{-3} Pa. During deposition, the total pressure was kept at 3.6 Pa. The O_2 (or N_2) / Ar ratio in the sputtering plasma was adjusted from 0 to 25 percent (vol.%); the films are noted as *SLTT-zO_2 or SLTT-zN_2*, with z the percentage of reactive gas in the sputtering plasma. The maximum N_2 fraction in discharge was limited to 25 vol.%, otherwise the deposited films deteriorate with delamination from the substrate. The films were all deposited with the target pre-sputtered in the same reactive gas percentage than the deposition, with the exception of the *SLTT-0N_2* sample deposited in pure argon from a target pre-sputtered with 0.95 vol.%N_2. The input power on the target was 90 W (power density: 2.0 W/cm^2). The temperature of the substrate holder (T_S) was set at 750°C during the deposition processes. The distance between substrate and target was fixed at 5 cm. After deposition, cooling was performed at 10°C.min^{-1} in the

deposition atmosphere. No post annealing was performed. The films were deposited on single-crystalline (001)MgO substrates; their deposition parameters and characteristics are given in Table 1.

Surface and cross-section observations were conducted using a JEOL 5440 Scanning Electron Microscope (SEM); error on thickness value is estimated as being lower than 25 nm. Visible transmittance spectra were carried out by a Perkin-Elmer Lambda 20 spectrometer operating in the range 200-1100 nm. The band-gap of the material (E_g) was extracted using the Kubelka-Munk formalism [25]; the error on the E_g value is estimated to be 0.05 eV. The chemical composition of samples was determined by semi-quantitative Energy Dispersive Spectrometry (EDS) in a JEOL 5440 SEM operating at 20 kV. The determination of the cationic Sr/Ta ratios was made using the $Sr_{K\alpha 1}$ (14,164 eV) and $Ta_{M\alpha 1}$ (1,710 eV) lines in order to avoid any overlapping. X-ray diffraction analyses were performed on a Seifert 3003 PTS diffractometer ($CuK_{\alpha 1}$ radiation). From the θ–2θ scans of the films, a Lotgering factor is calculated, defined as $F = P_F - P_P / 1- P_P$ [26], with ($_F$) relative to the compound in thin film form and ($_P$) in powder form, and $P = I_{110}/(I_{110} + I_{022})$ or $P = I_{004}/(I_{004} + I_{200})$ for oxide or oxynitride films, respectively (I_{hkl} : intensity of a (hkl) diffracted peak). This factor is used to quantitatively compare the orientation rates of different films; it can vary from 0 (non-orientation) to 1 (complete orientation). The mosaic spread of the crystallites around the direction of orientation was also characterized by the full width at half maximum ($\Delta\theta$) recorded in ω-scans. φ-scans were performed to verify the epitaxial growth of films.

3. RESULTS

3.1. Deposition rate

The sputtering deposition rate of the *SLTT-25O₂* film which is deposited with 25 vol.%O_2 in the discharge is equal to 45 nm/h. The deposition rate of the films deposited with

N_2 decreases with increasing dinitrogen concentration in the plasma as shown in Figure 1. Values decrease almost linearly from 450 nm/h for vol.%N_2 = 0 to 240 nm/h for vol.%N_2 = 5, and reach a plateau around 90 nm/h for vol.%N_2 = 21. Three factors can influence this decrease: first of all, the percentage of the main sputtering gas (here argon), second and third, the sputtering yield and the secondary electron emission yield of the target. It has been shown that the two latter are greater for nitride target compounds than for oxide target compounds [27,28]. The change in deposition rate can then be explained in relation with the poisoning of the oxide target when sputtered under dinitrogen. For low dinitrogen concentrations (i.e. vol.%$N_2 \leq 5$), the nitridation of the target is weak, so that the sputtering and secondary electron emission yields are those of an oxide target: the decrease of the deposition rate with increasing dinitrogen is explained by the simultaneous decrease of the argon content in the plasma. For moderate dinitrogen contents, the nitridation of target is high enough to begin to counteract the latter effect: the fall of the deposition rate is bent. For high dinitrogen concentrations (i.e. vol.$N_2 \geq 20$), the nitridation is nearly completed: a steady state is attained. Furthermore, the deposition rate of the oxidized target (45 nm/h with vol.%O_2 = 25) is actually much lower than that of the nitrited target (85 nm/h with vol.%N_2 = 25), in agreement with results from the literature [27,28].

3.2 Band gap and chemical composition

The band-gap values have been determined from the UV-Visible transmittance spectra. The evolution of E_g as a function of the dinitrogen percentage in the plasma is displayed in Figure 2. In accordance with its absorption in the UV region and its transparency, the band-gap of the *SLTT-25O₂* film is 4.75 eV. The *SLTT-0N₂* sample, deposited in pure argon from a "nitrided" target, is darkened compared to *SLTT-25O₂*, with a band-gap E_g = 3.65 eV. As soon as 1 vol.%N_2 is introduced in the sputtering plasma, the deposited film (*SLTT-1N₂)* shows an

absorption in the visible region with a yellowish coloration, and the band-gap abruptly decreases to E_g = 2.05 eV. For higher N_2 contents, the band-gaps remain around the same value (2.1 eV). The change of the band gap between oxide and oxynitride materials is explained by the fact that, due to their relative position in the periodic table of the elements, the electronic potential of N_{2p} orbitals is higher than O_{2p} orbitals. So, in an oxynitride where nitrogen is substituted for oxygen, the top levels of valence band are dominated by the N_{2p} orbitals and are elevated compared to an oxide. Since the metal d states stay mainly unchanged, this leads to the observed band gap narrowing.

The nitrogen content in films (at.%N_{film}) was probed by EDS (Table 1) and is shown in Figure 3 as a function of the dinitrogen percentage in the plasma. The at.%N_{film} varies from 0 for the *SLTT-0N₂* sample to 20 at.%, theoretical atomic percentage in the stoichiometric $(Sr_{0.99}La_{0.01})(Ta_{0.99}Ti_{0.01})O_2N$ compound, attained for vol.%$N_2 \geq 7$. For lower vol.%N_2, i.e. for *SLTT-1N₂*, *SLTT-3N₂* and *SLTT-5N₂* films, intermediate nitrogen contents are obtained (respectively, 10 at.%, 16.5 at.% and 16.5 at.%), despite band-gap values similar to the other films deposited under dinitrogen. As regards to the cations, the ratios Sr/Ta are close to 1 as shown in Table 1 and Figure 3, with the exception of the *SLTT-0N₂* sample with a ratio Sr/Ta = 0.55. No significant difference is seen between the N-containing samples; the *SLTT-25O₂* sample also presents a Sr/Ta ratio near 1.

3.3. Crystallization

The θ–2θ diffractograms of two representative samples (*SLTT-25O₂* and *SLTT-7N₂*) are given in Figure 4. The diffraction pattern of the sample deposited with O_2 can be indexed with the orthorhombic $Sr_2Ta_2O_7$ oxide (JCPDS 72-0921); nevertheless, a systematic angular deviation of diffracted peaks compared to tabulated values is noticed, which ranges from -0.59° for the first peak to -1.93° for the third one. The identification to other strontium

tantalates ($Sr_5Ta_4O_{15}$, hexagonal, isostructural to $Ba_5Ta_4O_{15}$ (JCPDS 72-0631); $SrTa_2O_6$, orthorhombic (JCPDS 77-0943)) has not been retained due to even greater angular deviations or to the absence of intense tabulated peaks. On (001)MgO substrate, the *SLTT-25O₂* film only shows {110} peaks (Lotgering factor F ≈ 1), with a value $\Delta\theta = 2.6°$ recorded on the (220) peak in ω-scan (Table 1). These results point out an (110) orientation of the film and additional φ-scan X-ray diffraction measurements were conducted to determine whether this sample was epitaxially grown on the MgO substrate. As for $Sr_2Ta_2O_7$, the crystallographic cell of $(Sr_{0.99}La_{0.01})_2(Ta_{0.99}Ti_{0.01})_2O_7$ is regarded as orthorhombic ($_O$), but it can also be considered as pseudo-cubic ($_{PC}$) since $a_O \sim c_O/\sqrt{2}$. The φ-scans were thus recorded around the $(101)_{PC}$ pole of the film and the (220) pole of the MgO substrate (Figure 5). One can see four peaks separated by 90° for the *SLTT-25O₂* sample, which depicts a four-fold symmetry cell in accordance with the hypothesis of a pseudo-cubic cell. The alignment of the films peaks to those of substrate demonstrates the epitaxial growth of the oxide film; the related epitaxial relationships are as follows: $(100)_{PCfilm}//(100)_{MgO}$ and $<001>_{PCfilm}//<001>_{MgO}$. In φ-scan, the full width at half maximum of the film peaks is $\Delta\varphi = 4.6°$, indicating a substantial dispersion of the crystallographic alignment.

The θ–2θ diffractogram of the *SLTT-7N₂* film is indexed with the tetragonal $SrTaO_2N$ oxynitride (JCPDS 79-1311), with nearly no angular deviation, for example +0.04° for the first peak. The {001} peaks are more intense than the others, indicating a preferred (001) orientation of the film. This is supported by a Lotgerin factor F = 0.534 and a value $\Delta\theta = 2.4°$ on the (004) peak (Table 1). The other films deposited under dinitrogen are all indexed in accordance with $SrTaO_2N$ with a preferred (001) orientation (Figure 6 and Table 1). The *SLTT-3N₂* and *SLTT-5N₂* samples may be considered as fully (001) oriented while the *SLTT-1N₂* sample presents the most polycrystalline growth. Furthermore, detailed diffractograms point out another difference between the N-containing samples. This consists in an angular

deviation of the diffracted peaks position towards higher 2θ values as the dinitrogen content in plasma increases. The films being (001) oriented, this corresponds to a decrease of the out-of-plane (c) parameter with increasing dinitrogen as shown in Figure 7, with a stabilization close to the bulk value of $SrTaO_2N$ (c_{bulk} = 8.0905 Å) for %vol.$N_2 \geq 7$. In the same time, the in-plane lattice parameter (a) values, deduced from θ–2θ patterns recorded at $\chi = 45°$, do not show significant change and remain practically constant around 5.725 Å, which is slightly higher than that of $SrTaO_2N$ bulk value (a_{bulk} = 5.692 Å). Considering the rather high thickness of studied films, one may consider that the observed decrease of the (c) parameter is not caused by a strain induced by the single-crystalline substrate, but rather by the deposition conditions, that is by the used dinitrogen percentage and consequently by the nitrogen content of films. In accordance with EDS results, we propose that depositions with vol.%$N_2 \geq 7$ lead to stoichiometric $(Sr_{0.99}La_{0.01})(Ta_{0.99}Ti_{0.01})O_2N$ whose lattice parameter (c) is close to 8.090 Å, while lower dinitrogen concentrations during deposition result in nitrogen-substoichiometric films with an elongation of the parameter (c). In both cases, the in-plane (a) parameter is unchanged, which suggests, for the $(Sr_{0.99}La_{0.01})(Ta_{0.99}Ti_{0.01})O_2N$ compound, a lattice (a) parameter close to 5.725 Å.

Besides these considerations, the highest Lotgering factor (F = 0.998) and narrowest Δθ peak (Δθ = 1.7°) are obtained for the film deposited at vol.%N_2 = 5 (Table 1). φ-scan measurements were conducted on *SLTT-3N₂*, *SLTT-5N₂* and *SLTT-7N₂* samples. For the latter two films, Figure 8 shows four peaks aligned with those of the substrate, which demonstrate the epitaxy of the films on MgO substrates. Nevertheless, the intensities for the *SLTT-7N₂* film are low and additional peaks spaced by 45° relative to the intense peaks are visible for *SLTT-5N₂* (and also for *SLTT-3N₂*). The latter denotes that two orientations of grains (rotated at 45° towards each other) coexist in the plane of these films. This is not observed for other oxynitrides films, so that it may be specific to the nitrogen-substoichiometric films showing

an elongated (c) parameter. For *SLTT-5N$_2$*, $\Delta\varphi = 8.0°$ and $\Delta\varphi = 19.6°$ values were recorded for the two type of peaks: the epitaxy on the MgO substrate may be considered as moderate.

Two indexations can be proposed for the *SLTT-0N$_2$* sample, deposited with 0 vol.%N_2 (see Supplementary data). First, it can be indexed through the $Sr_2Ta_2O_7$ oxide, with the same angular deviation than the *SLTT-25O$_2$* sample. In this case, *SLTT-0N$_2$* is polycrystalline with the occurrence of various (hkl) peaks and a Lotgering Factor F = 0.317. Second, considering its cationic ratio far beyond the other films (Sr/Ta = 0.55), one may envisaged a $SrTa_2O_6$ indexation and, in this case, the film presents a dual orientation, along the <201> and <002> directions, with Lotgering factors F' = 0.351 and F'' = 0.463, respectively.

3.4. Surface morphology

The surface morphologies of the two representative samples are shown in Figure 9. The oxide *SLTT-25O$_2$* sample presents a very smooth surface (Figure 8a), whereas fine rounded grains with diameter around 100 nm are observed for the *SLTT-7N$_2$* film (Figure 8b). The latter morphology is observed for the other oxynitride films except for the *SLTT-1N$_2$* film which presents random platelet acicular grains, approximately 500 nm in dimension (Figure 8c). This peculiar microstructure can be related to a more pronounced polycrystalline structure of the film as underlined by XRD. This type of morphology is seen on the *SLTT-0N$_2$* sample and can be related to its polycrystalline or dual oriented growth following the two possible indexations for this sample. No remarkable morphology has been observed for *SLTT-5N$_2$* (Figure 8d), in particular we did not notice any grains rotated at 45° as evidenced by XRD.

4. DISCUSSION

$(Sr_{0.99}La_{0.01})_2(Ta_{0.99}Ti_{0.01})_2O_7$ oxide film has been obtained through the combination of an "oxide" target and reactive O_2 in the sputtering plasma. The associated film (*SLTT-25O₂*) is transparent with a band-gap of 4.75 eV, epitaxially grown on MgO substrate and exhibits a homogeneous smooth surface. These features meet the results of the literature on $Sr_2(Nb_{1-x}Ta_x)_2O_7$ and undoped $Sr_2Ta_2O_7$ compounds. All studies involving these materials as thin films concern depositions on metallized-SiO_2/Si substrates and mainly for a use as high-κ gate dielectric. Fursenko reported a band-gap value (E_g = 4.6 eV) close to ours, for an amorphous film deposited by atomic vapor deposition on TiN/Si(001) substrate [23]. Polycrystalline $Sr_2(Nb_{0.1}Ta_{0.9})_2O_7$ and $Sr_2Ta_2O_7$ films have been obtained by Kim [17], Okuwada [18] and Kato [19] by chemical route depositions on Pt-SiO_2/Si substrates. Rodriguez [20] underlined the appearance of intense diffracted peaks on a $Sr_2Ta_2O_7$ film but he proposed a cubic cell with Pm3m space group (a = 3.955 Å) and indexed the peaks as {100} and {110}, in accordance with Rietveld structure refinement pointing out a cation deficiency. Our results are very similar to this study, but our interpretation is different as we rather believe, according to a hypothesis that Rodriguez himself proposed, that his sample was an orthorhombic film with a preferred orientation. As mentioned before, the orthorhombic cell of $(Sr_{0.99}La_{0.01})_2(Ta_{0.99}Ti_{0.01})_2O_7$ can be viewed as pseudo-cubic; taking into account the angular deviation in the θ–2θ diffractogram of sample *SLTT-25O₂*, the calculation gives a lattice parameter c_{PC} = 3.999 Å. In these conditions, the mismatch between the film and the MgO substrate (cubic, c = 4.211 Å) is - 5.0 %. This value explains the epitaxial growth of the *SLTT-25O₂* film on the MgO substrate. Yet, the mismatch is a few percent, so that the epitaxy of the film is moderate, as underlined by the value Δφ = 4.6°.

Concerning the oxynitrides, the EDS and XRD characterizations highlight the synthesis of two types of films. With the use of a nitrided target and for sufficient reactive N_2

gas amounts, i.e. when vol.%$N_2 \geq 7$, stoichiometric $(Sr_{0.99}La_{0.01})(Ta_{0.99}Ti_{0.01})O_2N$ films are obtained. They are colored with a band-gap of about 2.10 eV, present fine granular microstructures and are preferentially (001) oriented on (001)MgO substrate. The band gap is in perfect agreement with the value reported on pure $SrTaO_2N$ powders and crystals [4,29] and is close to the value E_g = 2.27 eV reported on thin films [24]. Nitrogen-substoichiometric films are deposited when using vol.%$N_2 \leq 5$. We assume that they crystallize in a $SrTaO_2N$-type tetragonal cell, slightly larger than the stoichiometric one.

Regarding the $(Sr_{0.99}La_{0.01})(Ta_{0.99}Ti_{0.01})O_2N$ cell as pseudo cubic, lattice parameters c_{PC} = 4.045 Å and a_{PC} = 4.048 Å are calculated. They do not evidence a tetragonal distortion as the one underlined by Oka on (001)-oriented and epitaxially films grown on Nb-doped $SrTiO_3$(001) substrates [24]. The mismatch with MgO substrate is - 3.9 %, low enough to explain the epitaxial growth of films; a dual orientation of the grains in the plane of the nitrogen sub-stoichiometric films has been evidenced.

The lack of variation of the band gap when dinitrogen is introduced in the sputtering plasma, underlined in Figure 2, is not in conflict with previous results. Changes are especially important for low nitrogen-content samples when looking to the studies on oxide/oxynitride solid solutions [30]. Here, EDS shows nitrogen contents already quite high in *SLTT-1N*$_2$ (10 at.%), *SLTT-3N*$_2$ (16.5 at.%) and *SLTT-5N*$_2$ (16.5 at.%) films. Changes in gap for these nitrogen contents are less pronounced because the top of the valence band is well defined by the high population levels associated with nitrogen. Moreover, we propose to consider the present oxynitride films as $(Sr,La)_n(Ta,Ti)_n(O,N)_{3n+2}$ compounds, in reference to $A_nB_nO_{3n+2}$ titanate, tantalate or niobate layered perovskite materials [31]. Assuming constant oxidation states for the cations, in particular for Ta (+V), the different n values will be attained by adjusting the oxygen and nitrogen contents, keeping the total anionic charge equal to -7 for electroneutrality. The nitrogen content will decrease as n decreases. The maximum nitrogen

content is related to n = ∞ and corresponds to the stoichiometric (Sr,La)(Ta,Ti)O_2N compound (i.e. (Sr,La)(Ta,Ti)$(O,N)_3$). This perovskite structure is made by infinite stack of (Ta,Ti)$(O,N)_6$ octahedra in the c direction. The minimum nitrogen content is related to n = 4 and corresponds to the (Sr,La)(Ta,Ti)$O_{3.5}$ oxide (i.e. $(Sr,La)_2(Ta,Ti)_2O_7$). In that case, the structure is made by the stack of four (Ta,Ti)O_6 octaedra separated by interlayers containing Sr (and La) and O atoms. In between, different n values may be envisaged for nitrogen containing materials and will correspond to the present nitrogen-substoichiometric films. In these compounds and for high enough n values, oxygen and nitrogen-containing interlayers repeat aperiodically and their XRD signature is that of a perovskite structure [31].

Finally, despite an intermediate band gap, XRD has not evidenced a mixture of oxide and oxynitride in the *SLTT-0N$_2$* sample; it is actually an oxide material. However, its darkening compared to the *SLTT-25O$_2$* film may indicate the presence of reduced metal species (Ta^{4+} or Ti^{3+}) resulting from anionic oxygen vacancies in the sample [32] arising from its deposition in pure argon. Further than the existence of unoccupied conduction levels in the band-gap, leading to a sub-band gap absorption and a darkening of the compound [33], here, the influence of the anion vacancies on the optical properties can be critical since the band-gap value of *SLTT-0N$_2$* (E_g = 3.65 eV) is also reduced compared to *SLTT-25O$_2$* (E_g = 4.75 eV).

In view of an integration of the oxide and oxynitride films in miniaturized and/or agile planar antennas, the next step of our study will be the measurement of the dielectric characteristics of films in low and high frequencies.

5. CONCLUSIONS

The objective of this study was to synthesize perovskite (Sr,La)-(Ta,Ti)-O-N oxide and oxynitride thin films. The formulation $(Sr_{0.99}La_{0.01})_2(Ta_{0.99}Ti_{0.01})_2O_7$ was synthesized as powder for the realization of a target for radio-frequency sputtering deposition. Films were

deposited with O_2 or N_2 rich plasmas at substrate temperature T_S = 750°C. The oxide $(Sr_{0.99}La_{0.01})_2(Ta_{0.99}Ti_{0.01})_2O_7$ film is transparent, with a band-gap E_g = 4.75 eV, and is (110) epitaxially grown on (001)MgO substrate. By varying dinitrogen percentage from 0 to 25 (%vol.) in the sputtering plasma, two kinds of oxynitride films are deposited. For vol.%$N_2 \geq$ 7, stoichiometric $(Sr_{0.99}La_{0.01})(Ta_{0.99}Ti_{0.01})O_2N$ films are produced, which are yellow with E_g ~ 2.10 eV and preferentially (001) oriented on (001)MgO substrate. For lower vol.%N_2, films display lower nitrogen contents and elongated out-of-plane lattice parameter. Among the oxynitrides, the best crystalline quality is obtained for vol.%N_2 = 5: the film is epitaxial, with the occurrence of two orientations in the plane of the film, rotated at 45° towards each other. Oxide and oxynitride (Sr,La)-(Ta,Ti)-O-N films are promising in order to achieve high permittivities, low dielectric losses and agility for a use in miniaturized and agile microwave devices.

REFERENCES

[1] F. Tessier, R. Marchand, Ternary and higher order rare-earth nitride materials: synthesis and characterization of ionic-covalent oxynitride powders, J. Solid State Chem. 171 (2003) 143-151.

[2] K. Maeda, D. Lu, K. Domen, Direct water splitting into hydrogen and oxygen under visible light by using modified TaON photocatalysts with d^0 electronic configuration, Chem. Eur. J. 19 (2013) 4986-4991.

[3] A.E. Maegli, S. Pokrant, T. Hisatomi, M. Trottmann, K. Domen, A. Weidenkaff, Enhancement of photocatalytic water oxidation by the morphological control of $LaTiO_2N$ and cobalt oxide catalysts, J. Phys. Chem. C, available online, dx.doi.org/10.1021/jp4084162.

[4] M. Jansen, H. P. Letschert, Inorganic yellow-red pigments without toxic metals, Nature 404 (2000) 980-982.

[5] R. Aguiar, D. Logvinovich, A. Weidenkaff, A. Rachel, A. Reller, S.G. Ebbinghaus, The vast colour spectrum of ternary metal oxynitride pigments, Dyes and Pigments 76 (2008) 70-75.

[6] Y. I. Kim, P.M. Woodward, K.Z. Baba-Kishi, C.W. Tai, Characterization of the structural, optical, and dielectric properties of oxynitride perovskites AMO_2N (A = Ba, Sr, Ca; M = Ta, Nb), Chem. Mater. 16 (2004) 1267-1276.

[7] Y-I. Kim, W. Si, P. M. Woodward, E. Sutter, S. Park, T. Vogt, Epitaxial thin-film deposition and dielectric properties of the perovskite oxynitride $BaTaO_2N$, Chem. Mater. 19 (2007) 618-623.

[8] Y-R. Zhang, T. Motohashi, Y. Masubuchi, S. Kikkawa, Sintering and dielectric properties of perovskite $SrTaO_2N$ Ceramics, J. Eur. Ceram. Soc. 32 (2011) 1269-1274.

[9] M. Yang, J. Oro-Sole, J. A. Rodgers, A. B. Jorge, A. Fuertes, J. P. Attfield, Anion order in perovskite oxynitrides, Nat. Chem. 3 (2011) 47-52.

[10] Y. Hinuma, H. Moriwake, Y.-R. Zhang, T. Motohashi, S. Kikkawa, I. Tanaka, First-principles study on relaxor-type ferroelectric behavior without chemical inhomogeneity in $BaTaO_2N$ and $SrTaO_2N$, Chem. Mater. 24 (2012) 4343-4349.

[11] L. Clark, J. Oro-Sole, K.S. Knight, A. Fuertes, J.P. Attfield, Thermally robust anion-chain order in oxynitride perovskites, Chem. Mater. 25 (2013) 5004-5011.

[12] D. Li, W. Li, C. Fasel, J. Shen, R. Riedel, Sinterability of the oxynitride $LaTiO_2N$ with perovskite-type structure, J. Alloys Comp. 586 (2014) 567-573.

[13] Y. Lu, C. Le Paven-Thivet, R. Benzerga, L. Le Gendre, A. Sharaiha, F. Tessier, F. Cheviré, Influence of the sputtering reactive gas on the oxide and oxynitride deposition by RF magnetron sputtering, Appl. Surf. Sci. 264 (2013) 533-537.

[14] Y. Lu, C. Le Paven, H. V. Nguyen, R. Benzerga, L. Le Gendre, S. Rioual, F. Tessier, F. Cheviré, A. Sharaiha, C. Delaveaud, X. Castel, Reactive sputtering deposition of perovskite

oxide and oxynitride lanthanum titanium films: structural and dielectric characterization, Crys. Growth Design 13 (2013) 4852-4858.

[15] S. Nanamatsu, M. Kimura, K. Doi, S.Matsushita, N. Yamada, A new ferroelectric: $La_2Ti_2O_7$, Ferroelectrics 8 (1974) 511-513.

[16] H. Yan, H. Ning, Y. Kan, P. Wang, M.J. Reece, Piezoelectric ceramics with super-high Curie points, J. Am. Ceram. Soc. 92 (2009) 2270-2275.

[17] C.Y. Kim, C.Y. Koo, D.C. Woo, H.Y. Lee, Ferroelectric $Sr_2(Nb,Ta)_2O_7$ thin films prepared by chemical solutiond, Jpn. J. Appl. Phys. 39 (2000) 5521-5524.

[18] K. Okuwada, S.-I. Nakamura, H. Nozawa, Crystal growth of layered perovskite $Sr_2Nb_2O_7$ and $Sr_2Ta_2O_7$ film by the sol-gel technique, J. Mater. Res. 14 (1999) 855-860.

[19] K. Kato, Surface morphology and dielectric properties of alkoxy-derived $Sr_2Ta_2O_7$ and $Sr_2(Ta,Nb)_2O_7$ thin films, J. Mater. Sci. Mater. Electr. 11 (2000) 575-578.

[20] M.A. Rodriguez, T.J. Boyle, B.A. Hernandez, D.R. Tallant, K. Vanheusden, A new metastable thin-film strontium tantalate perovskite, J. Am. Ceram. Soc. 82 (1999) 2101-2105.

[21] M. Lukosius, C. Wenger, S. Pasko, I. Costina, J. Dabrowski, R. Sorge, H.-J. Müssig, C. Lohe, Atomic vapour deposition of strontium tantalates films for MIM applications, IEEE Trans. Electr. Devices 55 (2008) 2273-2277.

[22] C.B. Kaynac, M. Lukosius, I. Costina, B. Tillack, C. Wenger, G. Ruhl, T. Blomberg, Enhanced leakage current behavior of $Sr_2Ta_2O_{7-x}/SrTiO_3$ bilayer dielectrics for metal–insulator–metal capacitors, Thin Solid Films 519 (2011) 5734-5739.

[23] O. Fursenko, J. Bauer, G. Lupina, P. Dudek, M. Lukosius, C. Wenger, P. Zaumseil, Optical properties and band gap characterization of high dielectric constant oxides, Thin Solid Films 520 (2012) 4532-4535.

[24] D. Oka,Y. Hirose, H. Kamisaka, T. Fukumura, K. Sasa, S. Ishii, H. Matsuzaki, Y. Sato, Y. Ikuhara, T. Hasegawa, Possible ferroelectricity in perovskite oxynitride $SrTaO_2N$ epitaxial thin films, Sci. Rep. 4 (2014) 4987.

[25] D. Kubelka, L. Munk, Ein beitrag zur optik der farbanstriche, Z. Tech. Phys. 12 (1931) 593-601.

[26] F.K. Lotgering, Topotactical reactions with ferrimagnetic oxides having hexagonal crystal structures, J. Inorg. Nucl. Chem. 9 (1959) 113-123.

[27] D.H. Kim, G.H. Lee, S.Y. Lee, D.H. Kim, Atomic scale simulation of physical sputtering of silicon oxide and silicon nitride thin films, J. Cryst. Growth 286 (2006) 71-77.

[28] D. Depla, X. Y. Li, S. Mahieu, R. De Gryse, Determination of the effective electron emission yields of compound materials, J. Phys. D: Appl. Phys. 41(2008) 202003-202007.

[29] Y. Mizuno, H. Wagata, K. Yubuta, N. Zettsu, S. Oishi, K. Teshima, Flux growth of $Sr_2Ta_2O_7$ crystals and subsequent nitridation to form $SrTaO_2N$ crystals, Cryst. Eng. Comm. 15 (2013) 8133-8138.

[30] F. Chevire, F. Tessier, R. Marchand, Optical properties of the perovskite solid solution $LaTiO_2N$–$ATiO_3$(A = Sr, Ba), Eur. J. Inorg. Chem. (2006) 1223-1230.

[31] F. Lichtenberg, A. Herrnberger, K. Wiedenmann, J. Mannhart, Synthesis of related layered $A_nB_nO_{3n+2}$ = ABO_x type niobates and titanates and their structural, electric and magnetic properties, Progr. Solid State Chem. 29 (2001) 1-70.

[32] M. Higashi, R. Abe, T. Takata, K. Domen, Photocatalytic overall water splitting under visible light using $ATaO_2N$(A = Ca, Sr, Ba) and WO_3 in a IO_3^-/I^- shuttle redox mediated system, Chem. Mater. 21 (2009) 1543-1549.

[33] S. Balaz, S. H. Porter, P. M. Woodward, L. J. Brillson, Electronic structure of tantalum oxynitride perovskite photocatalysts, Chem. Mater. 25 (2013) 3337-3343.

Table 1.
Deposition parameters and characteristics of $(Sr_{0.99}La_{0.01})$-$(Ta_{0.99}Ti_{0.01})$-O-N films deposited on MgO(001) substrate by reactive rf sputtering from a $(Sr_{0.99}La_{0.01})_2(Ta_{0.99}Ti_{0.01})_2O_7$ target at input power P = 90 W, total pressure p = 3.6 Pa and substrate temperature T_S = 750°C (the films were deposited with the target pre-sputtered in the same reactive gas percentage than the deposition, with the exception of the *SLTT-0N₂* sample deposited from a target pre-sputtered with 0.95 vol.%N_2).

Film	Reactive gas : vol.%	Thickness (nm)	Deposition rate (nm/h)	Band-gap E_g (eV)	at.% N_{film}	Sr/Ta	Δθ (°)	Lotgering factor
SLTT-25O₂	O_2 : 25	300	45	4.75	0	0.95	2.6	≈ 1
SLTT-0N₂	-	2125	450	3.65	0	0.55	4.4	0.317 (*0.351/0.463*)
SLTT-1N₂	N_2 : 1	2400	410	2.10	10	0.90	3.7	0.298
SLTT-3N₂	N_2 : 3	1800	300	2.10	16.5	0.90	3.0	0.995
SLTT-5N₂	N_2 : 5	1550	240	2.15	16.5	0.95	1.7	0.998
SLTT-7N₂	N_2 : 7	1300	215	2.15	19	0.85	2.4	0.534
SLTT-14N₂	N_2 : 14	900	160	2.05	20.5	0.90	2.1	0.686
SLTT-21N₂	N_2 : 21	420	90	2.10	20.5	1.10	2.6	0.511
SLTT-25N₂	N_2 : 25	1050	85	2.15	19	0.90	2.0	0.538

Highlights

- Oxide and oxynitride films were deposited by reactive RF magnetron sputtering
- $(Sr_{0.99}La_{0.01})_2(Ta_{0.99}Ti_{0.01})_2O_7$ film is (110) epitaxially grown on MgO substrate
- $(Sr_{0.99}La_{0.01})(Ta_{0.99}Ti_{0.01})O_2N$ films are preferentially (001) oriented on MgO substrate
- Nitrogen-substoichiometric films are deposited with low dinitrogen content in plasma

List of figure captions

Figure 1. Evolution of the deposition rate as function of the dinitrogen percentage in the sputtering plasma of $(Sr_{0.99}La_{0.01})(Ta_{0.99}Ti_{0.01})O_2N$ films deposited on (001)MgO substrates by reactive rf sputtering at T_S = 750 °C.

Figure 2. Evolution of the band-gap (E_g) as function of the dinitrogen percentage in the sputtering plasma of $(Sr_{0.99}La_{0.01})(Ta_{0.99}Ti_{0.01})O_2N$ films deposited on (001)MgO substrates by reactive rf sputtering at T_S = 750 °C.

Figure 3. Evolution of the nitrogen content (♦) and the Sr/Ta ratio (**x**) as a function of the dinitrogen percentage in the sputtering plasma of $(Sr_{0.99}La_{0.01})(Ta_{0.99}Ti_{0.01})O_2N$ films deposited on (001)MgO substrates by reactive rf sputtering at T_S = 750 °C (**Δ** is relative to the *SLTT-25O₂* sample deposited under $\%N_2 = 0$ and $\%O_2 = 25$).

Figure 4. θ–2θ X-ray diffractograms of the *SLTT-25O₂* and SLTT-7N_2 films deposited on (001)MgO substrate by reactive rf sputtering at T_S= 750 °C (films are labelled relatively to the nature and percentage of the reactive gas used in the sputtering plasma).

Figure 5. φ-scan X-ray diffractograms carried out for the $(101)_{PC}$ reflection of the *SLTT-25O₂* film (considering a pseudo cubic cell for the film material) and for the (220) reflection of the MgO substrate (the film is labelled relatively to the nature and percentage of the reactive gas used in the sputtering plasma).

Figure 6. θ–2θ X-ray diffractograms of the $(Sr_{0.99}La_{0.01})(Ta_{0.99}Ti_{0.01})O_2N$ films deposited on (001)MgO substrate by reactive rf sputtering at T_S= 750 °C (films are labelled relatively to the nature and percentage of the reactive gas used in the sputtering plasma).

Figure 7. Evolution of the out-of-plane (c) and in-plane (a) lattice parameters as function of the dinitrogen percentage in the sputtering plasma of $(Sr_{0.99}La_{0.01})(Ta_{0.99}Ti_{0.01})O_2N$ films deposited on (001)MgO substrates by reactive rf sputtering at T_S = 750 °C (the dotted lines are relative to the bulk $SrTaO_2N$ parameters: (c)-down and (a)-top).

Figure 8. φ-scan X-ray diffractograms carried out for the $(110)_{PC}$ reflection of the *SLTT-5N₂* and *SLTT-7N₂* films (considering a pseudo cubic cell for the film material) and for the (220) reflection of the MgO substrate (the films are labelled relatively to the nature and percentage of the reactive gas used in the sputtering plasma).

Figure 9. Surface SEM observations of the (a) *SLTT-25O₂*, (b) *SLTT-7N₂,* (c) *SLTT-1N₂* and (d) *SLTT-5N₂* films deposited on (001)MgO substrates by reactive rf sputtering at T_S= 750°C (films are labelled relatively to the nature and percentage of the reactive gas used in the sputtering plasma).

Figure 1

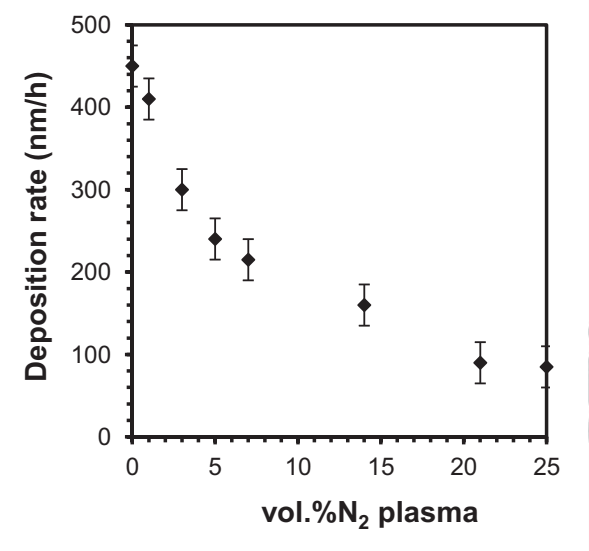

Figure 2

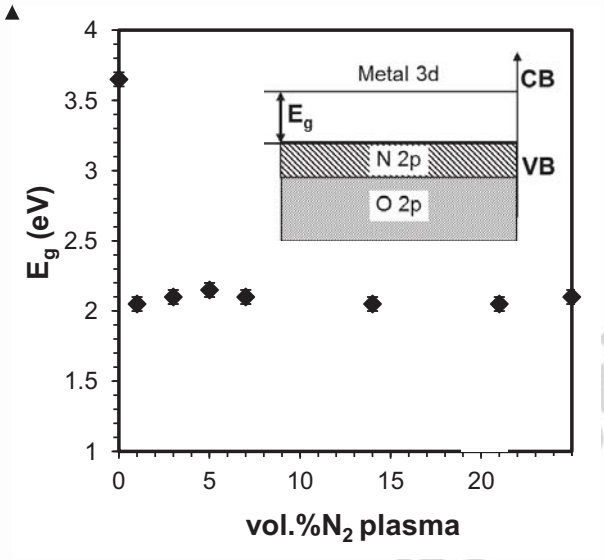

Figure 3

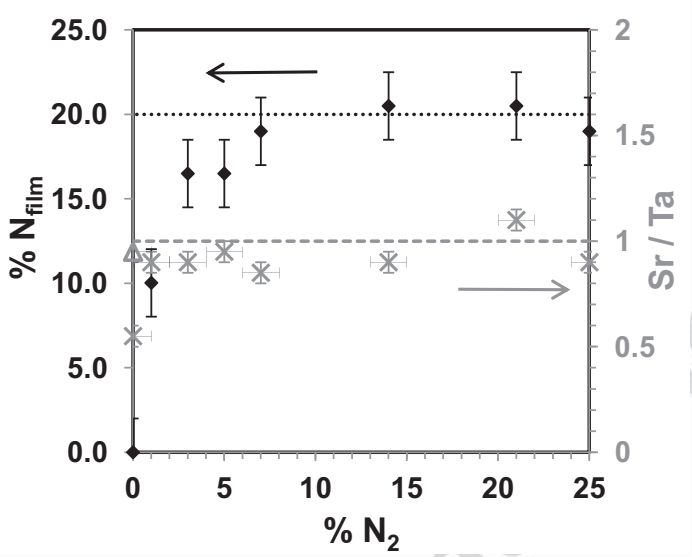

Figure 4

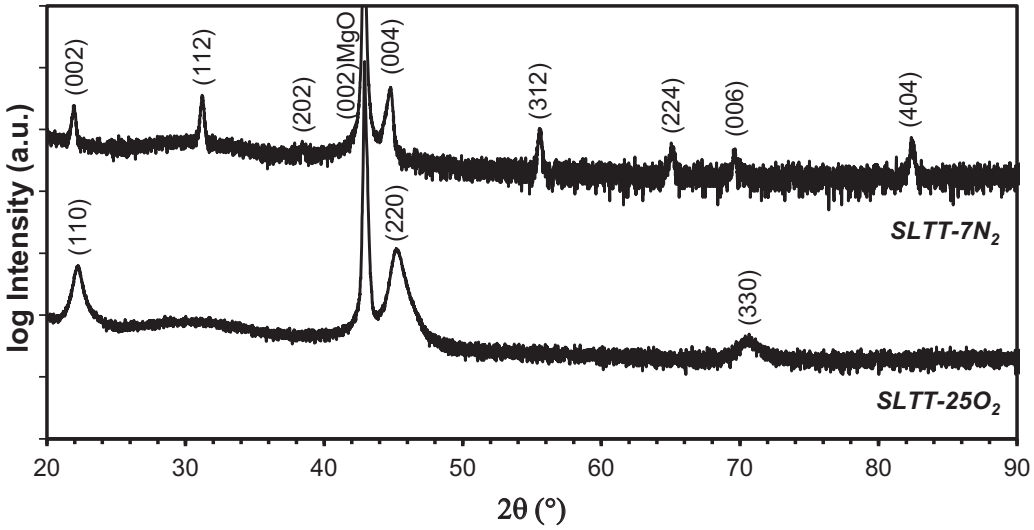

Figure 5

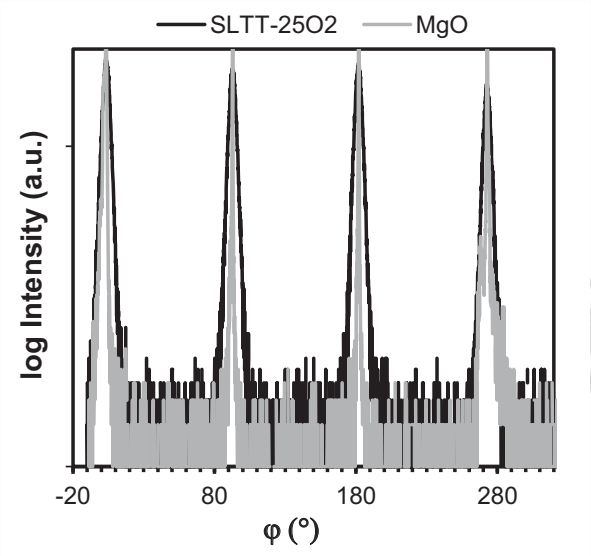

Figure 6

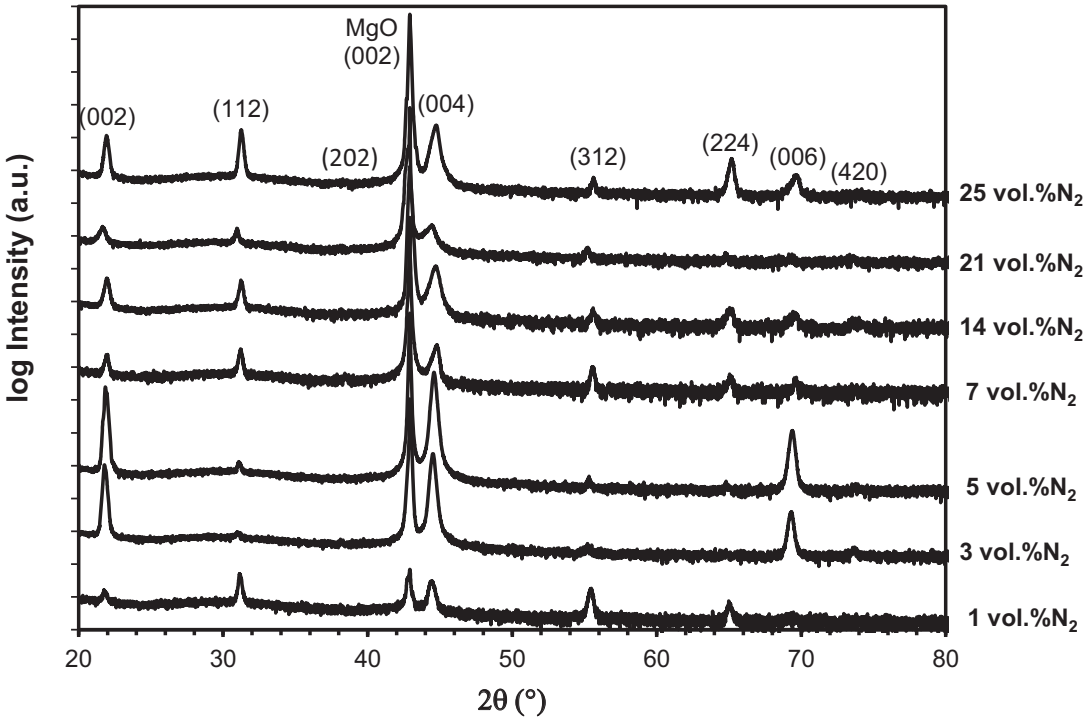

Figure 7

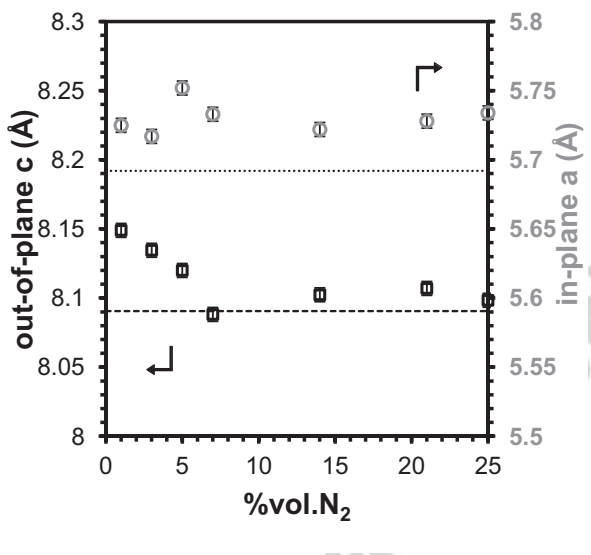

Figure 8

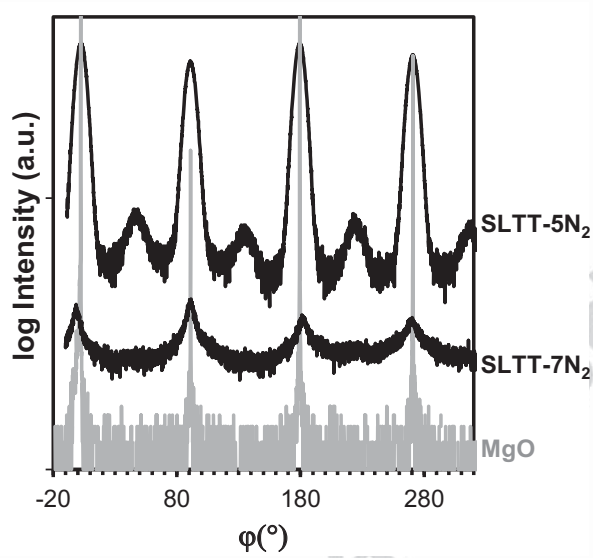

Figure 9